# Toward Lithium Ion Batteries with Enhanced Thermal Conductivity

Bonil Koo,[†] Pradyumna Goli,[§] Anirudha V. Sumant,[†] Paula Cecilia dos Santos Claro,[†,‖] Tijana Rajh,[†] Christopher S. Johnson,[‡] Alexander A. Balandin,[§] and Elena V. Shevchenko[†,*]

[†]Center for Nanoscale Materials and [‡]Chemical Sciences and Engineering, Argonne National Laboratory, Argonne, Illinois 60439, United States, [§]Nano-Device Laboratory, Department of Electrical Engineering and Materials Science and Engineering Program, Bourns College of Engineering, University of California, Riverside, California 92521, United States, and [‖] Instituto de Investigaciones Fisicoquímicas Teóricas y Aplicadas (INIFTA), Dpto de Química, FCE-UNLP, CONICET, La Plata 1900, Argentina

ABSTRACT As batteries become more powerful and utilized in diverse applications, thermal management becomes one of the central problems in their application. We report the results on thermal properties of a set of different Li-ion battery electrodes enhanced with multiwalled carbon nanotubes. Our measurements reveal that the highest in-plane and cross-plane thermal conductivities achieved in the carbon-nanotube-enhanced electrodes reached up to 141 and 3.6 W/mK, respectively. The values for in-plane thermal conductivity are up to *2 orders of magnitude* higher than those for conventional electrodes based on carbon black. The electrodes were synthesized *via* an inexpensive scalable *filtration* method, and we demonstrate that our approach can be extended to commercial electrode-active materials. The best performing electrodes contained a layer of γ-Fe$_2$O$_3$ nanoparticles on carbon nanotubes sandwiched between two layers of carbon nanotubes and had in-plane and cross-plane thermal conductivities of ∼50 and 3 W/mK, respectively, at room temperature. The obtained results are important for thermal management in Li-ion and other high-power-density batteries.
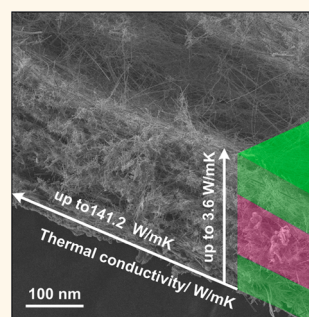
up to141.2 W/mK
Thermal conductivity/ W/mK
up to 3.6 W/mK
100 nm

O wing to their superior power density, Li-ion batteries are used in a wide variety of applications.[1] At the same time, this and similar types of batteries have a serious drawback, which is overheating and related safety concerns.[2] The heat is generated during the operation of any battery as current flows through the internal resistance of the battery whether it is being charged or discharged.[2,3] In the case of discharging, the temperature rise is limited by the energy stored in cathode material. No such limit exists in the charging cycle when energy can be pumped even after full charging of the battery.[3] In addition to Ohmic heating, chemical reactions that take place during charging and discharging in Li-ion batteries can also contribute to overheating. If overheating of the battery is not properly addressed, thermal runaway may cause a catastrophic destruction of the battery. From the other side, efficient heat removal from the battery allows for higher electrical currents to be achieved resulting in faster charging rates. These considerations explain the importance of thermal management

for operation and safety of any kind of high-power batteries.

There are a number of commonly used methods for removal of the excessive heat from the batteries, *e.g.,* increasing the air flow around the battery or maximizing the surface area of the electrodes.[4] It has been also shown that the thermal effects associated with Li-ion intercalation–deintercalation can be efficiently addressed by the certain combinations of the cathode and anode materials.[5] However, implementation of sophisticated engineered control methods for active cooling *via* enhanced air flow significantly increases the complexity of the battery design and its weight. The system level approaches cannot help with the localized hot spots and thermal gradients in the case of thick electrodes. The thermal and electrical gradients within the electrodes can lead to unbalanced charging and discharging resulting in lower energy storage capacity.[6]

Improving the thermal conductivity of the electrodes themselves is an essential step toward proper thermal management of the batteries. The latter is particularly important for Li-ion batteries because their

performance strongly depends on the electrode temperature.[7−9]

Conventional design of the electrodes involves mixing of the active materials with carbon black, conductive additives, and polymer binders that provide the integrity for the electrodes and electrical connectivity.[10] The problem with the carbon black-based electrodes, when used in high-power-density batteries, is their very low thermal conductivity of $K \sim 0.1–2$ W/mK at room temperature (rt).[11] Such low values stem from poor heat conduction properties of amorphous carbon, which is $K \sim 0.1–1$ W/mK near rt,[11,12] and the mechanical mix type structure of the electrodes, which introduces high thermal boundary resistance. The low thermal conductivity of the carbon black-based electrodes leads to their degradation as a result of the undesired thermally activated metal dissolution in cathodes or degradation of the surface electrolyte interface layer at anode.[13−15] Here, a *scalable* and *inexpensive* method for synthesis of the battery electrodes with significantly enhanced thermal conductivity is proposed.

Graphene and carbon nanotubes (CNTs) have the highest thermal conductivities of all known materials.[16−19] According to molecular dynamic calculations, the large phonon mean free paths in isolates single-walled CNT results in unusually high thermal conductivities up to $\sim$6600 W/mK at room temperature that is comparable to the thermal conductivity of an isolated graphene monolayer or graphite.[20] Experimentally, thermal conductivity of single-walled CNT was found to be in the range of 1750−5800 W/mK.[21] The thermal conductivity of individual multiwalled (MW) CNTs at room temperature can be as high as 3000 W/m K.[21] Thus, the thermal conductivities of CNTs are larger than the thermal conductivity of high-quality diamond crystals ($K \sim 2300$ W/mK)[22] that are used in semiconductor industry to prevent semiconducting materials from overheating.[23] However, unlike diamond, which is an electrical insulator, graphene and CNTs are electrical conductors and, as such, do not deteriorate electrical conductivity of composite materials. CNTs used as fillers were reported to improve the electrical conductivity of both anodes[24] and cathodes.[25] Recent studies indicated that CNTs and graphene can be also used as heat conducting fillers in composite materials.[26−29] Surface functionalization of CNTs, *e.g.,* attachment of certain chemical groups or nanoparticles, can improve their thermal coupling to the composite base material.[29] It was also demonstrated that CNTs by themselves can be used as the anode material in Li-ion batteries showing capacities up to 1000 mAh/g.[30] However, such electrodes suffer from large hysteresis in the voltage profiles between charge and discharge states and absence of the voltage plateau that limits their utilization in Li-ion batteries.[30]

RESULTS AND DISCUSSION

In the proposed approach, MW-CNTs were utilized as a matrix for encapsulation of electrochemically active cathode materials to fabricate electrodes for Li-ion batteries. The electrode material is prepared by the scalable and inexpensive *filtration* method, previously developed for sandwiching of nanometer-scale electrochemically active materials.[31,32] The filtration of the CNT suspension and the active cathode materials is carried out in isopropyl alcohol.[31] For the present study, a set of CNT-enhanced samples with variable layered structure were synthesized. The sample nomenclature and description are presented in Tables 1 and 2, correspondingly. The structures of the samples are illustrated in Figure 1.

Scanning electron microscopy (SEM) inspection indicates that the typical average thickness of the three-layered electrode—CNTs/cathode material/CNTs—is $\sim$140 μm (see Figure 2a). The average thickness of each CNT layer was determined to be $\sim$35 μm. The individual MW-CNTs were predominantly aligned parallel to the substrate. The latter has important implications for thermal transport. In addition to electrode materials that exhibited the best electrochemical performance, such as active material sandwiched between two layers of CNTs, thermal conductivity measurements for reference samples in different configurations were also performed (Figure 1). The variations in the sample layered structure and reference samples allowed the search for an optimum design

TABLE 1. Nomenclature of the Tested Samples

sample	layered structure	tests performed
NP-1	CNTs/{γ-Fe$_2$O$_3$ NPs on CNTs}/CNTs	battery capacity; in-plane K; cross-plane K
NP-2	CNTs/{γ-Fe$_2$O$_3$ NPs + CNTs}/CNTs	battery capacity; cross-plane K
NP-3	CNTs/{γ-Fe$_2$O$_3$ NPs + CNTs}	in-plane K; cross-plane K
NP-4	CNTs/γ-Fe$_2$O$_3$ NPs	in-plane K; cross-plane K
MP-1	CNTs/{Li[Ni$_{1/3}$Co$_{1/3}$Mn$_{1/3}$]O$_2$+CNTs}/CNTs	battery capacity; cross-plane K
MP-2	CNTs/{Li[Ni$_{1/3}$Co$_{1/3}$Mn$_{1/3}$]O$_2$+CNTs}	in-plane K; cross-plane K
REF-1	CNT bundle	cross-plane K

TABLE 2. Composition of the Tested Samples

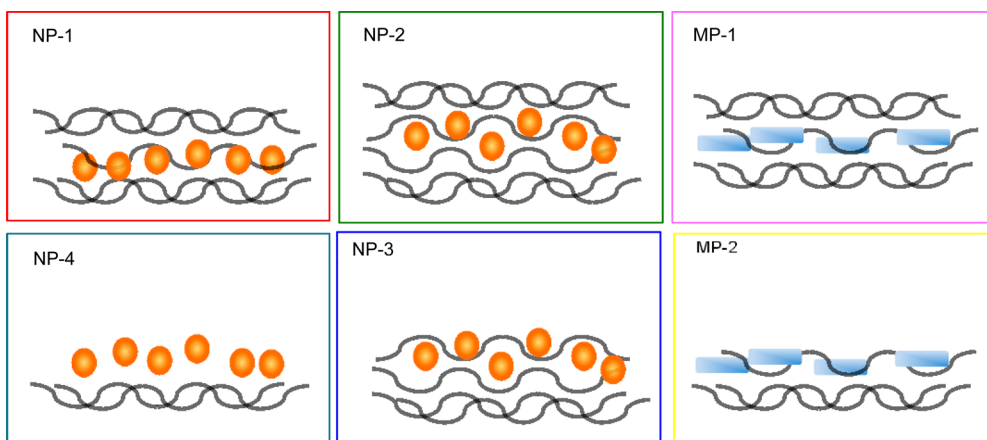| sample	layered structure	composition (mg)		
		layer 1	active layer	layer 2
NP-1	CNTs/{γ-Fe$_2$O$_3$ NPs on CNTs}/CNTs	4.5625	9.1250	4.5625
NP-2	CNTs/{γ-Fe$_2$O$_3$ NPs + CNTs}/CNTs	4.5950	9.9559	4.5950
NP-3	CNTs/{γ-Fe$_2$O$_3$ NPs + CNTs}	4.4582	9.4738	
NP-4	CNTs/γ-Fe$_2$O$_3$ NPs	4.5119	2.0271	
MP-1	CNTs/{Li[Ni$_{1/3}$Co$_{1/3}$Mn$_{1/3}$]O$_2$ + CNTs}/CNTs	4.5602	9.1205	4.5602
MP-2	CNTs/{Li[Ni$_{1/3}$Co$_{1/3}$Mn$_{1/3}$]O$_2$ + CNTs}	4.4618	9.9312	
REF-1	CNT bundle	10.002		

Figure 1. Schematic of the layered structure of the CNT enhanced battery electrodes. Dots and rectangles depict the hollow γ-Fe$_2$O$_3$ NPs and Li[Ni$_{1/3}$Co$_{1/3}$Mn$_{1/3}$]O$_2$ MPs, respectively. In sample NP-1, hollow γ-Fe$_2$O$_3$ NPs were synthesized on the surface of CNTs and sandwiched between two layers of CNTs. In samples NP-2, NP-3, MP-1, and MP-2, active particles were mixed with CNTs and further used to make a layer of active material. In sample NP-4, the layer of hollow γ-Fe$_2$O$_3$ NPs was deposited directed on the formed layer of CNTs. Vacuum filtration of corresponding solutions was applied to fabricate electrode structures.
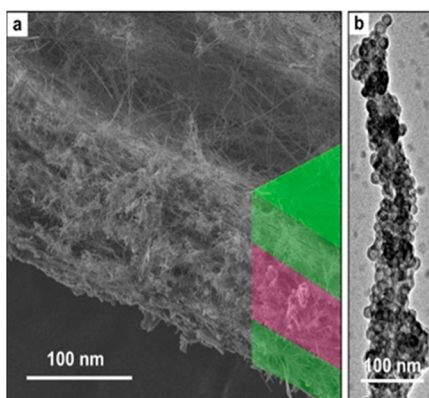

Figure 2. (a) Scanning electron microscopy image of the cross-section of the CNT enhanced battery electrodes. Note that CNTs are predominantly oriented along the sample plane. (b) Scanning electron microscopy image showing nanoparticles grown on CNTs.
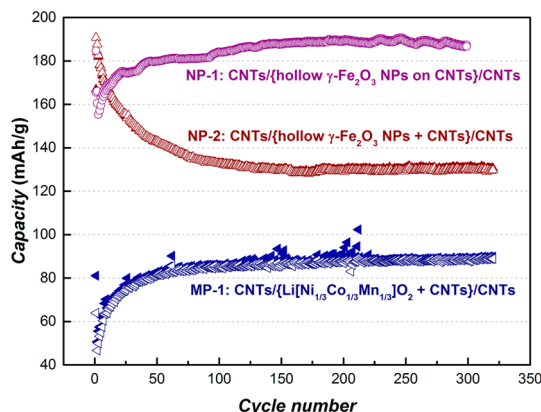

Figure 3. Charge (filled symbols) and discharge (open symbols) capacities versus cycle number for CNT-enhanced electrode structures. The cycling rate was 300 mA/g.

from the storage capacity and thermal management points of view.

One type of the electrodes contained the hollow γ-Fe$_2$O$_3$ nanoparticles (NPs) synthesized directly on CNTs (Figure 2b). The *hollow* NP refers to structures that have a void inside the iron oxide nanoshell. This void is formed as a result of the coalescence of the iron vacancies during the oxidation of iron.[33] The hollow γ-Fe$_2$O$_3$ NPs are ~15 nm large with ~4 nm thick shell. The γ-Fe$_2$O$_3$−NP-on-CNT layer was sandwiched between two layers of CNTs forming the CNTs/{γ-Fe$_2$O$_3$−NPs on CNTs}/CNTs structure. This structure was measured to have ~187 mAh/g capacity when cycled in cathode regime (4.5−1.5 V), excellent stability (no fading during 300 cycles), and 99.9% Coulombic efficiency (Figure 3). No current collectors were used in electrochemical tests. The results of the tests indicated that this electrode (sample NP-1) was the best in terms of its battery cathode performance.

The cycling of the electrode is accompanied by thermal effects, and heat removal may depend on the coupling between the CNTs and electrochemically active γ-Fe$_2$O$_3$ NPs. In order to study the effects of coupling of NPs and CNTs on the battery capacity and thermal conductivity, a sample where NPs were mixed with CNTs (not synthesized on them) was also analyzed. The mixed CNT-NP layer was sealed between two layers of CNTs forming CNTs/{hollow γ-Fe$_2$O$_3$ NPs + CNTs}/CNTs structure (sample NP-2). As seen in Figure 3, the electrochemical performance of these electrodes (capacity 130 mAh/g) was not as good as that of the electrodes that contained γ-Fe$_2$O$_3$ NP synthesized on CNTs (130 mAh/g vs 187 mAh/g).

A distinctively different type of electrode utilized Li[Ni$_{1/3}$Co$_{1/3}$Mn$_{1/3}$]O$_2$ microparticles (MPs).[34] The mixture of CNTs and Li[Ni$_{1/3}$Co$_{1/3}$Mn$_{1/3}$]O$_2$ MPs was sandwiched between two layers of CNTs by the filtration method forming CNTs/{Li[Ni$_{1/3}$Co$_{1/3}$Mn$_{1/3}$]O$_2$ + CNTs}/CNTs layers (sample MP-1). The thickness of the layers
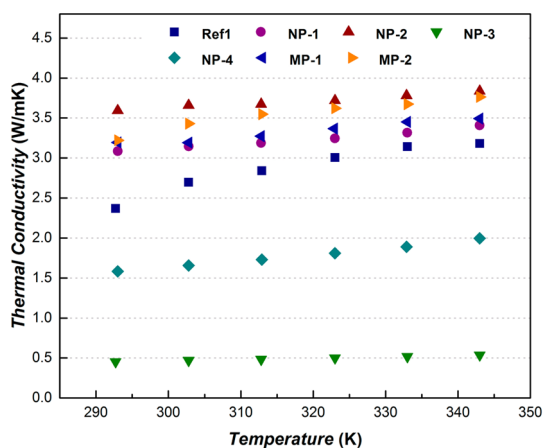
Figure 4. Cross-plane thermal conductivity for CNT enhanced electrode structures.

Figure 5. Comparison of the in-plane and cross-plane thermal conductivity of the CNT-enhanced battery electrodes at room temperature.

was similar to that in the NP-based electrodes. The electrochemical tests indicated that such electrodes have a lower capacity (Figure 3) as compared to electrodes fabricated via conventional approach.[30] However, their cycle stability was significantly higher. No capacity fading was observed up to 800 cycles while ~25−28% capacity loss after 50 cycles was reported for the same cathode material fabricated via a conventional method.[34] The capacity of this battery increased upon cycling up to 50 cycles and then stabilized. The stable performance is another attractive feature of CNT-enhanced electrode designs.

The thermal conductivity of the samples was determined using two different techniques: "laser flash" and "hot disk". Owing to the complicated structure of the samples and the "hot disk" equipment limitations, the in-plane thermal conductivity was measured at rt only. The cross-plane thermal conductivity was determined in the range from 290 to 350 K using the "laser flash" method. The details of the measurement procedures are given in the Experimental Section. The cross-plane thermal conductivity as a function of temperature for a set of examined electrodes is shown in Figure 4. The cross-plane thermal conductivity defines the heat transport through the electrode, i.e., perpendicular to the sample substrate. It can be seen that the cross-plane thermal conductivity values are in the range from ~0.5 to ~3.6 W/mK. Although the overall values are not significantly enhanced, many of them are higher than those in conventional electrodes.[11] The strong increase in cross-plane thermal conductivity is not expected because CNTs are predominantly oriented in-plane (along the substrate). In addition, the layered structure of the electrodes results in substantial thermal interface resistance between the layers, e.g., between the CNT layer and the {γ-Fe$_2$O$_3$ NPs + CNTs} layer or between the CNT layer and the substrate. The thermal conductivity increases slightly with the temperature or stays approximately constant. Such dependence is expected for material systems with large degree of disorder.
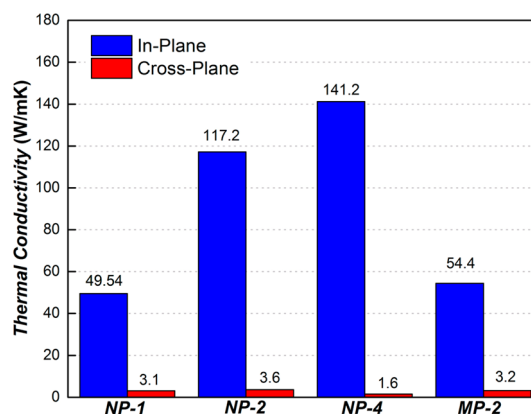
Figure 5 shows in-plane and cross-plane thermal conductivity for a set of different samples at rt. The in-plane thermal conductivity is substantially higher than the cross-plane conductivity. This is explained by the predominantly in-plane (along the substrate) orientation of CNTs. The in-plane values range from 50 to 141 W/mK. The NP-1 sample, which had the best electrochemical performance, revealed the thermal conductivity of 50 W/mK. This value is about 2 orders of magnitude higher than a thermal conductivity of the conventional carbon black-based electrodes[35] and at least two times higher than the in-plane thermal conductivity of the Sony Li-ion electrodes with engineered controls for heat removal such as copper current collector.[11]

Interestingly, the measured in-plane thermal conductivity values for these electrodes were typically even higher that the reported data for CNT bundles of the comparable thickness, i.e., $K \sim 15$ W/mK[36] that is likely to be attributed to differences in density and orientation of CNTs in the electrodes obtained by the filtration method. In fact, the thermal conductivity of NP-4 electrode, $K = 141$ W/mK, is by almost an order of magnitude higher than the values typically reported for the CNT bundles.[36] Such high thermal conductivity is most likely attributed to the sealing of CNTs during the filtration of the suspension of γ-Fe$_2$O$_3$ NPs.

The cross-plane thermal conductivity is in the range from 1.6 to 3.6 W/mK. The electrode with the best electrochemical performance revealed a thermal conductivity value of 3.1 W/mK at rt. This value is about 1 order of magnitude higher than that of the carbon black-based electrode materials.[35] It is also higher than the cross-sectional thermal conductivity of the electrodes of commercial Sony Li-ion batteries, i.e., 2.33 and 0.89 W/mK, for positive and negative electrodes, respectively.[11] The measured data indicate that all tested CNT electrodes revealed substantially enhanced in-plane and cross-plane thermal conductivities as compared to electrodes synthesized by the conventional

techniques, even though the enhancement is not as high as in the electrodes based on ordered CNT arrays.[12] However, the proposed electrodes were fabricated by the inexpensive scalable filtration method,[32] which can be extended to commercial electrode-active materials while the fabrication of ordered CNT arrays is still prohibitively expensive. The systematic study of thermal properties of CNT enhanced samples did not show a clear correlation with the specifics of the layered structure.

CONCLUSIONS

In conclusion, the thermal properties of Li-ion battery electrodes enhanced with multiwalled CNTs are reported. The electrodes were synthesized *via* an inexpensive scalable *filtration* method. The measurements indicate that the CNT enhanced electrodes reveal up to *2 orders of magnitude* enhancement of the thermal conductivity. The in-plane thermal conductivity in some electrodes reached ~141 W/mK at rt. The described approach for increasing the thermal conductivity can be extended to commercial electrode-active materials. The obtained results are important for thermal management of Li$^+$-ion and other high-power-density batteries. The proposed method of electrode fabrication could allow further improvements of the thermal conductivity of the electrode structures in Li-ion batteries by incorporation of graphene or diamond nanoparticles.

EXPERIMENTAL DETAILS AND METHODS

Materials Synthesis and Electrochemical Testing. The CNTs used in this work were purchased from Aldrich (≥95% purity, product and CAS nos. are 636487 and 308068-56-6, respectively). The dimensions (o.d. × i.d. × L) of multiwalled CNTs were 20−30 nm × 5−10 nm × 0.5−200 μm, respectively. Hollow γ-Fe$_2$O$_3$ NPs and γ-Fe$_2$O$_3$ NPs on CNTs were synthesized according the synthetic protocols described in ref 32. In order to fabricate CNT-based electrodes 4.0 mg of multiwalled CNTs was dispersed in 150 mL of isopropyl alcohol (IPA) and sonicated for 5 min. After that, the suspension of CNTs was filtrated by vacuum through the filter (microporous polyolefin separator Celgard 2325) that served as a separator in electrochemical tests. As a result, a black paper made of CNTs was formed onto the filter. The active layer was fabricated in the same manner: 12.0 mg of electrode material (hollow γ-Fe$_2$O$_3$ NPs or Li[Ni$_{1/3}$Co$_{1/3}$Mn$_{1/3}$]O$_2$) mixed with 3 mg of CNTs in IPA was vacuum-filtrated forming a uniform layer. In the case of hollow γ-Fe$_2$O$_3$ NPs synthesized on the surface of CNTs, 15 mg of the material that contained 12.0 mg of γ-Fe$_2$O$_3$ NPs and 3 mg of CNTs were used (see Table 2 for sample composition details). After the evaporation of the solvent residue, the CNT-based composite electrodes were annealed in an oven at 200 °C for 12 h and further used in electrochemical tests without any additional processing. The TEM and SEM inspection of the samples was carried out using JEOL 2100F and JEOL 7500F instruments, respectively. The electrochemical tests were performed with the 2032 coin type cells with Li metal foil as the counter electrodes and 1.2 M LiPF$_6$ in ethylene carbonate/ethyl methyl carbonate (3:7 weight ratio) electrolyte (Tomiyama). Half-cell cycles were operated at 300 mA/g between 4.5−1.5 V *vs* Li/Li$^+$ using an automated Maccor battery tester at ambient temperature. The voltage range for hollow γ-Fe$_2$O$_3$ NPs and Li[Ni$_{1/3}$Co$_{1/3}$Mn$_{1/3}$]O$_2$ were 4.5−1.5 and 4.5−2.0 V, respectively.

Thermal Measurements. The cross-plane thermal conductivity was measured using a noncontact optical "laser flash" technique (Netzsch LFT). LFT is a transient method that directly measures thermal diffusivity. In order to perform LFT measurements, each sample was placed into a special stage, a xenon flash lamp produced shots with an energy of 10 J/pulse on the sample surface, while the temperature rise was measured at the other end with an InSb infrared (IR) detector. The thermal conductivity was determined from the equation $K = \rho \alpha C_p$, where ρ is the mass density of the sample and C_p is the specific heat of the sample measured with Netzsch instrument separately. The in-plane thermal conductivity of the samples was measured using the transient planar source (TPS) technique (Hot Disk TPS2500). For these measurements, an electrically insulated flat nickel sensor with a radius of 0.5 mm is sandwiched between two identical parts of the same sample. The sensor acted as the heat source and temperature monitor simultaneously.[37−39] The surfaces of the specimens were flattened and cleaned to reduce the thermal conduct resistance at the sensor-sample surfaces. Thermal properties of the material are determined by recording the temperature rise as a function of time using the equation $\Delta T(\tau) = P(\pi^{(3/2)} rK)^{-1} D(\tau)$, where $\tau = (t_m \alpha / r^2)^{1/2}$, α is the thermal diffusivity, t_m is the transient measurement time, r is the radius of the sensor, P is the input heating power, and $D(\tau)$ is the modified Bessel function. The time and the input power are chosen so that the heat flow is within the sample boundaries and the temperature rise of the sensor is not influenced by the outer boundaries of the sample.[37−39]

REFERENCES AND NOTES

1. Aricò, A. S.; Bruce, P.; Scrosati, B.; Tarascon, J.-M.; van Schalkwijk, W. Nanostructured Materials for Advanced Energy Conversion and Storage Devices. *Nat. Mater.* **2005**, *4*, 366–377.
2. Linden, D.; Reddy, T. B. *Handbook of Batteries*, 3rd ed.; McGraw-Hill: New York, 2002.
3. Spotnitz, R.; Franklin, J. Abuse Behavior of High-Power, Lithium-Ion Cells. *J. Power Sources* **2003**, *113*, 81–100.
4. Bitsche, O.; Gutmann, G. Systems for Hybrid Cars. *J. Power Sources* **2004**, *127*, 8–15.
5. Viswanathan, V. V.; Choi, D.; Wang, D.; Xu, W.; Towne, S.; Williford, R. E.; Zhang, J.-G.; Liu, J.; Yang, Z. Effect of Entropy Change of Lithium Intercalation in Cathodes and Anodes on Li-Ion Battery Thermal Management. *J. Power Sources* **2010**, *195*, 3720–3729.
6. Garimella, S. V.; Fleischer, A. S.; Murthy, J. Y.; Keshavarzi, A.; Prasher, R.; Patel, C.; Bhavnani, S. H.; Venkatasubramanian, R.; Mahajan, R.; Joshi, Y.; et al. Thermal Challenges in Next-Generation Electronic Systems. *IEEE Trans. Compon. Packag. Technol.* **2008**, *31*, 801–815.
7. Amatucci, G. G.; Schmutz, C. N.; Blyr, A.; Sigala, C.; Gozdz, A. S.; Larcher, D.; Tarascon, J. M. Materials' Effects on the Elevated and Room Temperature Performance of CLiMn$_2$O$_4$ Li-Ion Batteries. *J. Power Sources* **1997**, *69*, 11–25.
8. Zhang, S. S.; Xu, K.; Jow, T. R. Electrochemical Impedance Study on the Low Temperature of Li-Ion Batteries. *Electrochim. Acta* **2004**, *49*, 1057–1061.

9. Ji, Y.; Zhang, Y.; Wang, C.-Y. Li-Ion Cell Operation at Low Temperatures. *J. Electrochem. Soc.* **2013**, *160*, A636–A649.

10. Fransson, L.; Eriksson, T.; Edström, K.; Gustafsson, T.; Thomas, J. O. Influence of Carbon Black and Binder on Li-Ion Batteries. *J. Power Sources* **2001**, *101*, 1–9.

11. Maleki, H.; Hallaj, S. A.; Selman, J. R.; Dinwiddie, R. B.; Wang, H. Thermal Properties of Lithium-Ion Battery and Components. *J. Electrochem. Soc.* **1999**, *146*, 947–954.

12. Evanoff, K.; Khan, J.; Balandin, A. a.; Magasinski, A.; Ready, W. J.; Fuller, T. F.; Yushin, G. Towards Ultrathick Battery Electrodes: Aligned Carbon Nanotube-Enabled Architecture. *Adv. Mater.* **2012**, *24*, 533–537.

13. Vetter, J.; Novák, P.; Wagner, M. R.; Veit, C.; Möller, K. C.; Besenhard, J. O.; Winter, M.; Wohlfahrt-Mehrens, M.; Vogler, C.; Hammouche, A. Ageing Mechanisms in Lithium-Ion Batteries. *J. Power Sources* **2005**, *147*, 269–281.

14. Bandhauer, T. M.; Garimella, S.; Fuller, T. F. A Critical Review of Thermal Issues in Lithium-Ion Batteries. *J. Electrochem. Soc.* **2011**, *158*, R1–R25.

15. Ramadass, P.; Haran, B.; Gomadam, P. M.; White, R.; Popov, B. N. Development of First Principles Capacity Fade Model for Li-Ion Cells. *J. Electrochem. Soc.* **2004**, *151*, A196–A203.

16. Balandin, A. A. Thermal Properties of Graphene and Nanostructured Carbon Materials. *Nat. Mater.* **2011**, *10*, 569–581.

17. Nika, D. L.; Askerov, A. S.; Balandin, A. A. Anomalous Size Dependence of the Thermal Conductivity of Graphene Ribbons. *Nano Lett.* **2012**, *12*, 3238–3244.

18. Nika, D. L.; Balandin, A. A. Two-Dimensional Phonon Transport in Graphene. *J. Phys.: Condens. Matter* **2012**, *24*, 233203.

19. Shahil, K. M. F.; Balandin, A. A. Thermal Properties of Graphene and Multilayer Graphene: Applications in Thermal Interface Materials. *Solid State Commun.* **2012**, *152*, 1331–1340.

20. Berber, S.; Kwon, Y.-K.; Tománek, D. Unusually High Thermal Conductivity of Carbon Nanotubes. *Phys. Rev. Lett.* **2000**, *84*, 4613–4616.

21. Kim, P.; Shi, L.; Majumdar, A.; McEuen, P. L. Thermal Transport Measurements of Individual Multiwalled Nanotubes. *Phys. Rev. Lett.* **2001**, *87*, 215502.

22. Anthony, T. R.; Banholzer, W. F.; Fleischer, J. F.; Wei, L.; Kuo, P. K.; Thomas, R. L.; Pryor, R. W. Thermal Diffusivity of Isotopically Enriched ^{12}C Diamond. *Phys. Rev. B* **1990**, *42*, 1104–1111.

23. Goyal, V.; Sumant, A. V.; Teweldebrhan, D.; Balandin, A. A. Direct Low-Temperature Integration of Nanocrystalline Diamond with GaN Substrates for Improved Thermal Management of High-Power Electronics. *Adv. Funct. Mater.* **2012**, *22*, 1525–1530.

24. Endo, M.; Kim, Y. A.; Hayashi, T.; Nishimura, K.; Matusita, T.; Miyashita, K.; Dresselhaus, M. S. Vapor-Grown Carbon Fibers (VGCFs): Basic Properties and Their Battery Applications. *Carbon* **2001**, *39*, 1287–1297.

25. Sotowa, C.; Origi, G.; Takeuchi, M.; Nishimura, Y.; Takeuchi, K.; Jang, I. Y.; Kim, Y. J.; Hayashi, T.; Kim, Y. A.; Endo, M.; et al. The Reinforcing Effect of Combined Carbon Nanotubes and Acetylene Blacks on the Positive Electrode of Lithium-Ion Batteries. *ChemSusChem* **2008**, *1*, 911–915.

26. Shahil, K. M. F.; Balandin, A. A. Graphene-Multilayer Graphene Nanocomposites as Highly Efficient Thermal Interface Materials. *Nano Lett.* **2012**, *12*, 861–867.

27. Goyal, V.; Balandin, A. A. Thermal Properties of the Hybrid Graphene-Metal Nano-Micro-Composites: Applications in Thermal Interface Materials. *Appl. Phys. Lett.* **2012**, *100*, 073113.

28. Goli, P.; Legedza, S.; Dhar, A.; Salgado, R.; Renteria, J.; Balandin, A. A. Graphene-Enhanced Hybrid Phase Change Materials for Thermal Management of Li-Ion Batteries. *J. Power Sources* **2014**, *248*, 37–43.

29. Gulotty, R.; Castellino, M.; Jagdale, P.; Tagliaferro, A.; Balandin, A. A. Effects of Functionalization on Thermal Properties of Single-Wall and Multi-Wall Carbon Nanotube-Polymer Nanocomposites. *ACS Nano* **2013**, *7*, 5114–21.

30. Baughman, R. H.; Zakhidov, A. A.; de Heer, W. A. Carbon Nanotubes--the Route toward Applications. *Science* **2002**, *297*, 787–792.

31. Koo, B.; Chattopadhyay, S.; Shibata, T.; Prakapenka, V. B.; Johnson, C. S.; Rajh, T.; Shevchenko, E. V. Intercalation of Sodium Ions into Hollow Iron Oxide Nanoparticles. *Chem. Mater.* **2013**, *25*, 245–252.

32. Koo, B.; Xiong, H.; Slater, M. D.; Prakapenka, V. B.; Balasubramanian, M.; Podsiadlo, P.; Johnson, C. S.; Rajh, T.; Shevchenko, E. V. Hollow Iron Oxide Nanoparticles for Application in Lithium Ion Batteries. *Nano Lett.* **2012**, *12*, 2429–2435.

33. Cabot, A.; Puntes, V. F.; Shevchenko, E.; Yin, Y.; Balcells, L.; Marcus, M. A.; Hughes, S. M.; Alivisatos, A. P. Vacancy Coalescence During Oxidation of Iron Nanoparticles. *J. Am. Chem. Soc.* **2007**, *129*, 10358–10360.

34. Myung, S.-T.; Lee, K.-S.; Yoon, C. S.; Sun, Y.-K.; Amine, K.; Yashiro, H. Effect of AlF$_3$ Coating on Thermal Behavior of Chemically Delithiated Li$_{0.35}$[Ni$_{1/3}$Co$_{1/3}$Mn$_{1/3}$]O$_2$. *J. Phys. Chem. C* **2010**, *114*, 4710–4718.

35. Song, L.; Evans, J. W. Measurements of the Thermal Conductivity of Lithium Polymer Battery Composite Cathodes. *J. Electrochem. Soc.* **1999**, *146*, 869–871.

36. Yang, D. J.; Zhang, Q.; Chen, G.; Yoon, S. F.; Ahn, J.; Wang, S. G.; Zhou, Q.; Wang, Q.; Li, J. Q. Thermal Conductivity of Multiwalled Carbon Nanotubes. *Phys. Rev. B: Condens. Matter* **2002**, *66*, 165440.

37. Gustafsson, S. E.; Karawacki, E.; Chohan, M. A. Thermal Transport Studies of Electrically Conducting Materials Using the Transient Hot-Strip Technique. *J. Phys. D: Appl. Phys.* **1986**, *19*, 727.

38. Gustafsson, S. E. Transient Plane Source Techniques for Thermal Conductivity and Thermal Diffusivity Measurements of Solid Materials. *Rev. Sci. Instrum.* **1991**, *62*, 797.

39. Gustafsson, M.; Wang, H.; Trejo, R. M.; Lara-Curzio, E.; Dinwiddie, R. B.; Gustafsson, S. E. On the Use of the Transient Hot-Strip Method for Measuring the Thermal Conductivity of High-Conducting Thin Bars. *Int. J. Thermophys.* **2006**, *27*, 1816–1825.